

Cite this: *Digital Discovery*, 2026, 5,  
583

## When machine learning models learn chemistry II: applying WISP to real-world examples

Kerrin Janssen,<sup>a</sup> Jan M. Wollschläger,<sup>ib</sup> Jonny Proppe<sup>\*a</sup> and Andreas H. Göller<sup>id</sup><sup>\*c</sup>

In our previous work, we introduced WISP (Workflow for Interpretability Scoring using matched molecular Pairs), which enables users to quantitatively assess the performance of explainability methods for machine learning models. In this work, we focus on more complex tasks, such as yield prediction,  $pK_i$  values for inhibition of coagulation Factor Xa and AMES mutagenicity, where the explanations of the predicted property need to capture more intricate interaction patterns between structural motifs of either the reaction partner, the protein or DNA. Expanding upon part I of the “When Machine Learning Learns Chemistry” series, we demonstrate additional functionalities of the WISP workflow. Alongside the model and descriptor-agnostic atom attributor, WISP integrates a SHAP-based and an RDKit-based attribution method, enabling the comparison of multiple explainability approaches, as demonstrated on the Factor Xa dataset. This work also showcases WISP’s capability to evaluate explanations for classification tasks such as AMES mutagenicity. The application of WISP to the AMES mutagenicity dataset reveals that the respective machine learning model fails to learn the underlying chemical relationships, instead relying primarily on numerical correlations. When applied to the yield dataset, WISP highlights specific cases where explainability methods that usually perform well fail to provide meaningful insights. This highlights WISP’s ability to detect such limitations in trained models, providing valuable insights to guide targeted improvements in model development and data quality.

Received 5th September 2025  
Accepted 5th December 2025

DOI: 10.1039/d5dd00399g

rsc.li/digitaldiscovery

### 1 Introduction

By providing meaningful explanations for predictions of machine learning models, these models can be leveraged to guide molecular design decisions in the life sciences.<sup>1–3</sup> This is often achieved in the form of heatmaps that highlight the contributions of individual molecular atoms, indicating whether they influence a property of interest positively or negatively (Fig. 1).<sup>4–9</sup> Such visualizations can be valuable to both machine learning experts and non-experts.<sup>5,10</sup> For example, in computer-aided synthesis planning, such explanations can help identify functional groups that lower reaction yields, allowing chemists to replace them with more favorable alternatives.<sup>11,12</sup> In drug design, they can pinpoint molecular regions that reduce bioactivity or increase toxicity, which can then be modified or removed to improve a compound’s properties.<sup>13,14</sup>

A key limitation of current explainability methods in chemistry is that single-atom attributions often lack chemical plausibility, making it difficult to trust or interpret the explanations meaningfully. For example, highlighting a single carbon atom

within a phenyl ring provides no actionable insight, as this does not reflect the delocalized electronic nature of the system or inform any chemically sensible design choices a chemist could make. To address this issue, we proposed WISP (a Workflow for Interpretability Scoring using matched molecular Pairs) to evaluate XAI attribution schemes.<sup>15</sup> To evaluate the atom attributions produced by the explainability methods, we applied the concept of matched molecular pairs (MMPs). By comparing atom attributions specifically on the variable and constant parts of MMPs, this approach ensures that any structural change assessed is chemically meaningful and interpretable. Since modifications within an MMP are inherently chemically plausible, this method provides a robust basis for validating whether atomic contributions align with established chemical structure–property relationships.<sup>16</sup>

In part I of the “When Machine Learning Models Learn Chemistry” series, we introduced WISP as a model- and descriptor-agnostic tool to quantify the chemical explainability capabilities of machine learning models.<sup>15</sup> Using datasets with well-defined physicochemical properties, we demonstrated how WISP can help identify robust models that are capable of providing reliable explanations for unseen data.<sup>15</sup>

In this work, we apply WISP to tasks relevant for computer-aided synthesis planning and drug discovery, demonstrating its application to more complex endpoints. We highlight the implications of these findings for model and dataset

<sup>a</sup>TU Braunschweig, Institute of Physical and Theoretical Chemistry, Gauss Str 17, 38106 Braunschweig, Germany. E-mail: j.proppe@tu-braunschweig.de<sup>b</sup>Bayer AG, Pharmaceuticals, R&D, Machine Learning Research, 13353 Berlin, Germany<sup>c</sup>Bayer AG, Pharmaceuticals, R&D, Computational Molecular Design, 42096 Wuppertal, Germany. E-mail: andreas.goeller@bayer.com

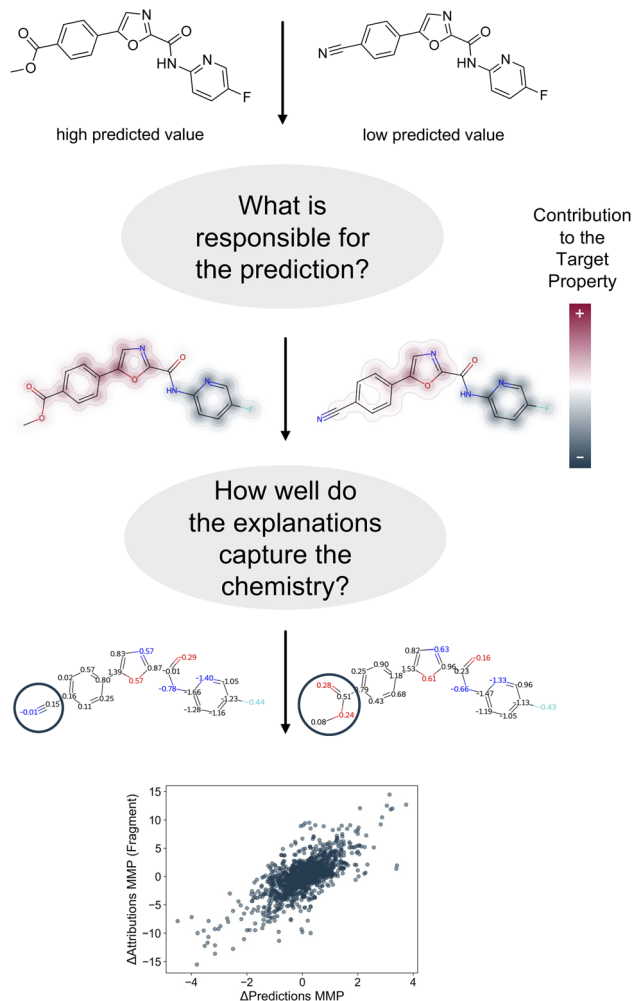


Fig. 1 The predicted molecules (top) can be analyzed and visualized as heatmaps (middle), which illustrate the contribution of each atom to the predicted outcome. To assess how well these heatmaps capture the underlying chemistry, we evaluate the attributions within the variable part of the MMPs (circled regions in the bottom molecules). This approach provides a quantitative measure of the explainability performance (bottom).

development and discuss how insights into explainability can inform decision-making in life sciences.

## 2 Methods

### 2.1 Datasets

To evaluate the explainability performance on a dataset relevant to computer-aided synthesis planning, we used a dataset containing liquid chromatography area percent (LCAP) yields.<sup>11,17</sup>

Table 1 Datasets and resulting MMPs used in this work

Dataset	Type	#	# after prep.	# MMPs	Source
Merck US	LCAP yields	264	264	46	17
Sanofi FXa	pK <sub>i</sub> on Factor Xa	1068	938	2042	18
Ames mutagenicity	Classification on AMES test	6130	6127	5616	19

These yields stem from a mild, functional-group-tolerant synthesis protocol developed by Felten *et al.*, which involves the carboxylation of 1,3-azoles followed by an amide coupling step.<sup>17</sup> With 264 LCAP yields, this is the smallest dataset used in this work (Table 1).

For the domain of drug design, we employed two datasets: one consisting of 1068 pK<sub>i</sub> values for inhibition of coagulation Factor Xa, and another containing 6130 AMES mutagenicity measurements (Table 1).<sup>18,19</sup>

For the preprocessing, we applied the same standardizing protocol as in our previous work:<sup>15</sup>

- Filter molecules to maximally 1000 atoms.
- Enumerate up to 10 tautomers for canonicalization.
- Retain only the largest fragment per SMILES.
- Perform normalization and sanitization.
- Remove SMILES duplicates with conflicting experimental target values; keep one entry when targets agree.

This uniform preprocessing ensures that all molecular representations are standardized and comparable.

### 2.2 WISP specifications

In this work, we also made use of several additional features included in WISP. The general workflow of WISP is described in detail in part I of this series. It includes a preprocessing step followed by model training, supporting both various scikit-learn models and chemprop models. Subsequently, attributions are calculated and evaluated using matched molecular pairs (MMPs).

WISP supports the evaluation of model explanations for classification tasks. To this end, it integrates a training routine that combines Morgan fingerprints with a random forest classifier, which we applied here to the AMES dataset. To enable the same explainability assessment as for regression tasks, the model outputs are provided as class probabilities. The maximum heatmap color intensity is set to 0.7 in this case.

In the Python version of WISP, unlike in the web application, users can also include a pre-trained model within the workflow. This option is particularly valuable for machine learning users with specific requirements for model training that fall outside the scope of WISP's built-in routines. We demonstrate this feature using the LCAP dataset.

In addition to the atom attributor, WISP integrates two further explainability methods.<sup>15</sup> While these methods are less generally applicable than the atom attributor, their integration allows for a direct comparison of different explainability approaches within the WISP framework.

**2.2.1 Atom attributor.** As described in part I of the “When Machine Learning Learns Chemistry” series, we applied the



atom attributor in this work. This method estimates atomic contributions by systematically mutating the respective atoms in the input SMILES strings, thereby quantifying each atom's influence on the model's prediction.<sup>15</sup> Because this approach relies solely on SMILES-based perturbations, it is model- and descriptor-agnostic, making it broadly applicable to a wide range of machine learning models commonly used in the life sciences.

**2.2.2 SHAP attributor.** The SHapley Additive exPlanations (SHAP) method is widely used to interpret model predictions.<sup>5,11,20–22</sup> The calculation of SHAP values involves iteratively training models with one feature removed at a time and measuring the change in predictions relative to the original, full-feature model.<sup>23</sup> When combined with Morgan fingerprints as input features, these feature importances can be mapped back onto the molecular structure to generate atom-level attributions. While SHAP values can be computed for a wide variety of models, generating atom-level attributions depends on using input features that encode atom-level information.

**2.2.3 RDKit attributor.** One attribution method implemented in RDKit is available in the SimilarityMaps module as GetAtomicWeightsForModel.<sup>24</sup> This approach developed by Riniker and Landrum is model-agnostic and works with both Morgan and RDK fingerprints.<sup>24</sup> The method determines atom attributions by identifying the fingerprint bits set by the atom of interest, removing those bits, and recalculating the model prediction using the modified fingerprint.<sup>24</sup> One limitation of this method is that potential bit collisions can influence the attributions, which may partly explain why this explainability approach sometimes fails to capture the effects of specific functional groups.<sup>24</sup> Bit collisions occur when multiple structural motifs are hashed into the same bit in the fingerprint.

## 3 Results and discussion

### 3.1 Model performances

In this study, we employed the machine learning model previously trained and evaluated on a dataset of 264 liquid chromatography area percent (LCAP) yields, published by Felten *et al.*<sup>11,17</sup>

The models for Factor Xa and AMES were trained entirely within the WISP workflow, resulting in models based on Morgan fingerprints and a random forest architecture (Table 2).<sup>18,19</sup>

### 3.2 LCAP yield

Yield prediction plays an important role in computer-aided synthesis planning (CASP).<sup>25</sup> It helps conserve resources and significantly reduces time requirements.<sup>25</sup>

Since this model is trained on RDKit path-based fingerprints, the atom attribution method and the RDKit attribution method can be applied. However, the WISP workflow does not include an evaluation of train-test dependency when a pre-trained model is provided, as is the case here.

For this model, the atom-based explanations over the entire molecule yield a relatively high correlation with the predicted differences, with an  $r^2$  of 0.92 (Table 3). However, this correlation drops significantly when considering only the variable part of the MMP, as shown in Table 3. This drop in performance is primarily due to MMPs where a nitrile group is replaced with a methyl ester (Fig. 2, middle), which deviates notably from the previously observed correlation of the other MMP attributions with the predictions. However, such an imbalance does not seem to affect other transformations, such as the exchange of a methoxy group for a hydrogen atom (Fig. 2, bottom), where the MMP exchange shows no apparent influence on the prediction,

**Table 2** Model performances on the test set. LCAP yield and Factor Xa are regression models, AMES is a classification model.  $r^2$  denotes the squared Pearson correlation coefficient between experimental values and predictions,  $AE_{\max}$  refers to the maximum absolute error, and CM indicates the confusion matrix

Property of interest	Model type	$r^2$	MAE	RMSE	$AE_{\max}$	Model source
LCAP yield	RDKit fingerprint; Bayesian ridge	0.69	7.4	9.9	23.6	11
Factor Xa	Morgan fingerprint; random forest	0.63	0.52	0.73	2.43	WISP
Property of interest	Model type	Accuracy	Precision	Recall	CM	Model source
AMES	Morgan fingerprint; random forest	0.80	0.79	0.80	406 141 110 568	WISP

**Table 3** Performance of the explainability methods on the LCAP yield dataset

Attribution method	$r^2$ whole molecule to pred.	$r^2$ variable part to pred.	$r^2$ whole molecule to LCAP yield	Std constant part	Accuracy variable part to pred.
Atom attributions	0.92	0.51	0.25	3.02	0.89
RDKit attributions	0.87	0.37	0.10	2.78	0.70



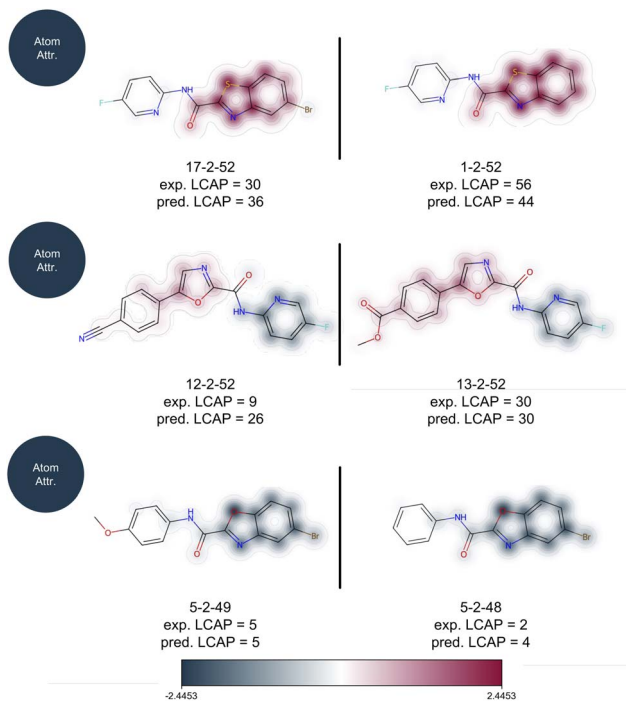


**Fig. 2** Comparison of the heatmaps for three different MMPs from the LCAP dataset, generated using the atom attributor within WISP and scaled uniformly for consistency. A negative attribution, shown in blue, indicates a decreasing influence on the predicted property, whereas a positive attribution, shown in red, reflects an increasing influence.

a trend that is consistently reflected in the explainability results. These findings suggest that, while uncritical for most transformations, the model does not capture the underlying chemistry of specific transformations and their influence on reaction yield. This demonstrates how WISP can highlight regions where the model's explanations may lack chemical validity, providing valuable insight into the extent to which these explanations should inform design decisions. Moreover, this information can be used to systematically improve models or datasets in areas where the current model fails to capture the underlying chemistry, ultimately supporting the development of more robust and reliable predictive models in the future.

Another limitation of the atom-based attribution is its lack of alignment with actual experimental outcomes. The  $r^2$  between the  $\Delta\text{attributions}_{\text{MMP}}$  of the whole molecule and the experimental yield reaches only 0.25, which cannot be considered a meaningful correlation (Table 3). This implies that the model's explanations are unsuitable for guiding experimental design in general. Therefore, the explainability methods are only capable of capturing the predictions to a limited extent and fail to generalize to the true property of interest. This suggests that the model did not learn the underlying chemistry but instead relied mainly on numerical correlations in the input data. The small standard deviation in the constant part suggests that the model has captured consistent patterns, though not the underlying chemistry itself. Given that the LCAP dataset is purely combinatorial, this result is not entirely unexpected. All

these aspects highlight the inherent difficulty of yield prediction as a task.<sup>26</sup>

Looking into the classifying results, we feel that qualitatively, the atom attribution method still appears to perform well (Table 3). This is primarily due to the fact that most of the  $\Delta\text{attributions}_{\text{MMP}}$  and the corresponding prediction differences fall within the negative range. As a result, even flawed regions are classified as false negatives, which artificially inflates the accuracy. In effect, these instances contribute positively to the overall accuracy despite introducing underlying attribution errors. This issue could potentially be mitigated by employing larger or more balanced datasets.

The quantitative performance of the RDKit attribution method is similarly poor as that of the atom attributor (Table 3). In this case, the lack of correlation is further emphasized by the clear separation of different MMP transformations, which prevents the formation of a coherent explainability–prediction relationship. The lower region of the correlation plot (Fig. SI-1b) corresponds to transformations where a bromine atom is replaced with hydrogen (Fig. 2, top); the central region includes nitrile-to-methyl ester transformations (Fig. 2, middle); and the upper region reflects methoxy-to-hydrogen substitutions (Fig. 2, bottom). As with the RDKit-based attribution method, the atom attributor fails to differentiate sufficiently between the two molecules involved in the nitrile-to-methyl ester transformation. Visual inspection of the attributions reveals that the variable part of the MMP receives low attribution values (Fig. 2, middle). The underlying cause is the sparse bit coverage in the fingerprint representation of these bonds, with only 36 bits for 12-2-43 and 38 for 13-2-43. In contrast, other bonds are associated with 70 to 369 bits. This indicates that an attribution value close to zero in the RDKit method does not necessarily imply a low contribution to the model's explanation but may instead reflect a sparsity in fingerprint coverage.

This demonstrates how WISP can be applied to external models to evaluate their explainability and to identify instances where the model fails to capture the underlying chemistry. However, it is important to note that the dataset used in this analysis comprises only 46 MMPs (Table 1), which limits the statistical robustness and generalizability of the conclusions drawn. Accordingly, the size of this dataset may indicate a lower limit for the practical application of WISP. However, the exact requirement on dataset size will vary based on the specific structural characteristics of the dataset in question.

### 3.3 Factor Xa

In adaptation of the work by Harren *et al.*, we evaluated the explainability methods on a dataset of bioactivity values for coagulation Factor Xa.<sup>22</sup> As the original dataset was not publicly available, the authors recommended the dataset used by Bailey *et al.* as a comparable alternative.<sup>18</sup>

When evaluating the qualitative performance of the explainability methods, all approaches perform overall comparably (Table 4). For whole-molecule explanations, the SHAP attributor shows a slight advantage, whereas the RDKit attributor performs best when focusing on the variable part.



Table 4 Accuracy of  $\Delta$ attributions MMP versus  $\Delta$ predictions MMP for  $pK_i$  values of Factor Xa inhibitors

Attribution method	Whole molecule training set	Variable part training set	Whole molecule test set	Variable part test set
Atom attributions	0.91	0.84	0.76	0.72
RDKit attributions	0.89	0.84	0.80	0.80
SHAP attributions	0.94	0.80	0.85	0.74

To obtain a quantitative measure, we correlate the  $\Delta$  in MMP attributions with the  $\Delta$  in model predictions using the squared Pearson correlation coefficient. Across all three attribution methods, the explanations for the whole molecule are well-correlated with the predictions, showing high squared Pearson correlation coefficients:  $r^2 = 0.91$  (atom),  $r^2 = 0.89$  (RDKit), and  $r^2 = 0.93$  (SHAP) (Table 5,  $r^2$  whole molecule to pred.). The performance of the explanations for the training values is similarly strong (Table 5). For the variable part of the MMPs, the  $r^2$  drops to 0.66 for the atom attributor and to 0.65 for the RDKit attributor, and to 0.57 for SHAP (Table 5). Nonetheless, these values remain relatively high in comparison to other endpoints evaluated in this and the previous study.<sup>15</sup> The standard deviation in the attributions of the constant part is 15.78 for the atom attributor and 15.17 for the RDKit attributor—placing them in the bottom compared to previous models. The SHAP attributor achieves a notably lower standard deviation of 7.36. Although some strong outliers are visible in the data, the overall trend suggests reliable and consistent performance of the explainability methods across attribution types.

**3.3.1 Comparison with Harren *et al.*** To evaluate the explainability approaches used in this work, we compared our findings on Factor Xa to established explainability methods. This analysis serves to verify the reliability of the attributors employed here and to prevent incorrect conclusions arising from a flawed explainability technique. An unreliable explainability method might create the false impression that a well-performing model has not successfully learned important

chemical relationships. The models used in the work by Harren *et al.* were trained on 318 data points for the smaller version and 3160 for the larger one.<sup>22</sup> In this work, 1068 data points were used (Table 1). With a test set squared Pearson  $r^2$  of 0.56 for the smaller and 0.76 for the larger model, our model's performance, with an  $r^2$  of 0.63 (Table 2), lies between these two reported in the reference paper.<sup>22</sup> This should be considered when comparing the results.

In Fig. 3, the heatmaps for structure 873, generated by all three explainability methods, are shown. This structure corresponds to compound 3 in the study by Harren *et al.*<sup>22</sup> The predicted  $pK_i$  of our model for this compound is 6.28 (weak activity), which falls between the values predicted by the models in Harren *et al.* (6.20 and 6.38).<sup>22</sup> This trend is also reflected in the heatmaps: the isopropyl group and the tertiary nitrogen are indicated as having a neutral influence by both the atom attributor and the RDKit attributor, while the SHAP attributor suggests a slight positive influence for the isopropyl group (Fig. 3). Since the azetidine motif is generally less favored compared to larger substituents in this position, the model explanations appear to capture this subtle structural context well, in contrast to the heatmaps presented by Harren *et al.* for the larger dataset.<sup>22</sup>

Another example is an MMP discussed by Harren *et al.*<sup>22</sup> In this case, the variable part is an exchange of a bromine atom for an iodine atom (Fig. 4). The structure containing the bromine has the higher  $pK_i$ , while the structure with the iodine shows a lower  $pK_i$ . This difference should be reflected in the

Table 5 Overview of the performance of the explainability methods. The best results in each column are shown in bold, and the worst results are shown in italics. POI stands for property of interest

Attribution method	POI	Training set				Test set	
		$r^2$ whole molecule to pred.	$r^2$ variable part to pred.	$r^2$ whole molecule to POI	Std constant part	Accuracy variable part to pred.	$r^2$ whole molecule to POI
Atom attributor	Crippen $\log P$	0.73	0.79	0.66	<b>2.85</b>	0.90	0.64
	Exp. $\log P$	<i>0.61</i>	0.61	<i>0.49</i>	4.95	0.83	0.41
	Solubility	0.85	<b>0.90</b>	0.78	4.32	<b>0.94</b>	<b>0.77</b>
	Factor Xa	0.91	0.66	<b>0.92</b>	<i>15.78</i>	0.84	0.08
	AMES	0.84	0.66	0.86	14.61	<i>0.71</i>	0.09
RDKit attributor	Factor Xa	0.89	0.65	0.91	15.17	0.84	0.07
	AMES	0.67	<i>0.53</i>	0.71	13.82	0.73	<i>0.04</i>
SHAP attributor	Factor Xa	<b>0.93</b>	0.57	0.87	7.36	0.80	0.09
Corr.:	—	-0.14	<b>0.60</b>	<i>-0.47</i>	<b>0.79</b>	<b>0.54</b>	<b>1.0</b>



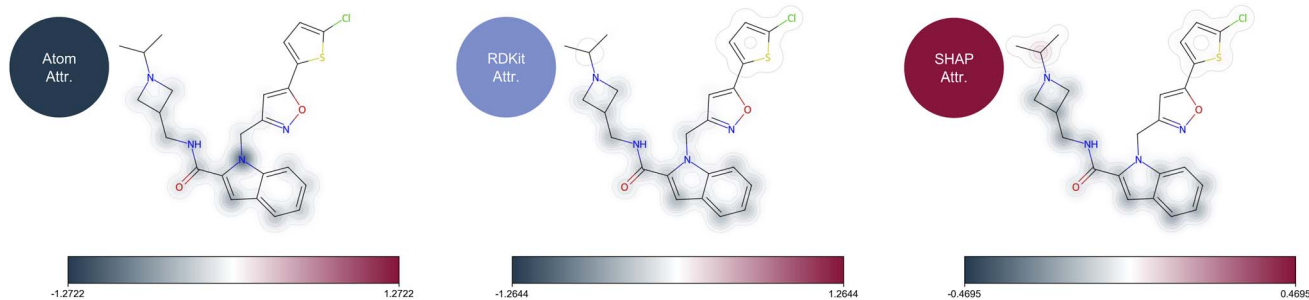


Fig. 3 Comparison of the heatmaps for structure 873 from the Factor Xa dataset. This molecule is part of the training set and has an experimental  $pK_i$  of 6.08 and a predicted  $pK_i$  of 6.27.

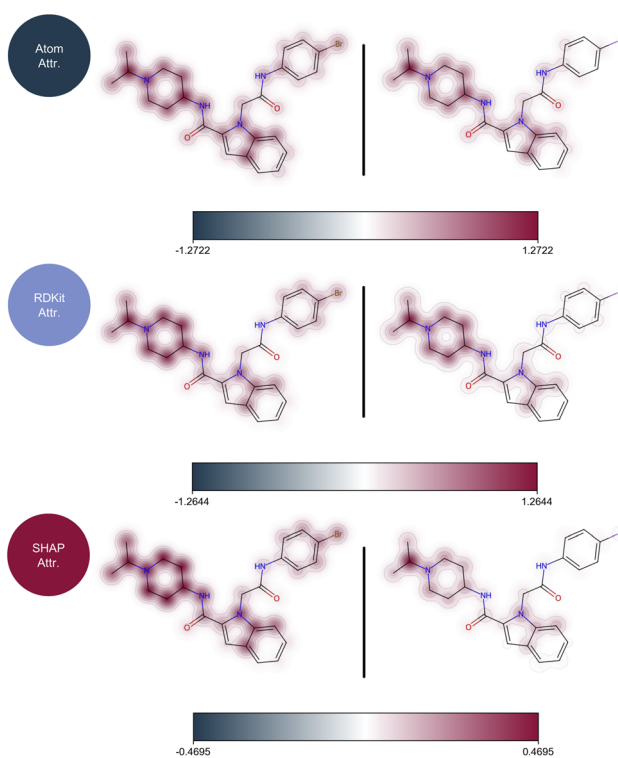


Fig. 4 Comparison of the heatmaps for structure 83 (left) and structure 375 (right). Both structures are part of the training set. Structure 83 has an experimental  $pK_i$  of 8.50 and a predicted  $pK_i$  of 8.12, while structure 375 has an experimental  $pK_i$  of 7.64 and a predicted  $pK_i$  of 7.63.

attributions and, consequently, in the heatmaps. Indeed, the bromine is highlighted as having a positive influence, whereas the iodine shows a neutral influence (Fig. 4). This result contrasts with the findings of Harren *et al.*, where their model explanation did not correctly attribute the variable part of this MMP, despite using their better-performing model for the analysis.<sup>22</sup>

This is also reflected in the quantitative assessment of the explainability methods on the Factor Xa dataset, where the atom attributor achieves the highest squared Pearson correlation coefficient for property of interest explanations on the training set across all datasets examined in this study (Table 5). This outcome further validates both the atom attributor and the

WISP workflow, demonstrating strong alignment between the qualitative insights from the heatmaps and the quantitative results—both of which are supported by the experimental reference data. Additionally, this analysis highlights the critical importance of careful dataset curation: if specific functional group effects are to be learned by the model, the necessary variations must be well represented in the underlying data.

### 3.4 AMES

The AMES mutagenicity dataset represents a complex challenge, since the model must learn to recognize non-additive toxicophores—structural motifs that are known to cause mutagenicity but whose effects do not simply add up linearly.<sup>27</sup> As AMES is the only classification task in this study, it poses an additional challenge to the WISP framework. Because for a classification problem, there are four discrete types of property changes associated with each MMP ( $A, B$ ):  $A_0 \mapsto B_0 (\Delta = 0)$ ,  $A_1 \mapsto B_1 (\Delta = 0)$ ,  $A_0 \mapsto B_1 (\Delta = 1)$ ,  $A_1 \mapsto B_0 (\Delta = -1)$ , but only three of these are distinguishable in the plot (Fig. SI-2 and SI-3a, b). This is because both in the case of two negatives and two positives, the same difference ( $\Delta = 0$ ) is obtained. From an application perspective, these MMP types include pairs where the transformation leads from mutagenic to non-mutagenic ( $\Delta = -1$ ), from non-mutagenic to mutagenic ( $\Delta = 1$ ), or results in no change in mutagenicity ( $\Delta = 0$ ). Consequently, the original binary classification problem with discrete targets  $y_{\text{target}} \in \{0, 1\}$  and predictions  $y_{\text{pred}} \in \{0, 1\}$ , once transformed into the MMP framework of WISP, turns into an ordinary regression. As we judged squared errors to remain sensible within this setting (*e.g.* a  $-1/1$  mistake is four-times more costly compared to a  $0/1$  mistake), it was decided to remain evaluating with the  $r^2$  on the predicted probability output of the model. A further advantage of this approach is its consistency with the regression endpoints, allowing us to compare the explainability performances on whole molecule and variable part (Table 5) to the other observations made.

However, these distinctions disappear when examining the test set, which already indicates that the model may not generalize well. The variance in the constant part is in the same range as for the Factor Xa dataset, with a standard deviation of 14.61 for the atom attributor and 13.82 for the RDKit attributor (Table 5). On the test set, the atom attributor shows generally



good explainability performance. However, the explanations do not appear to correlate strongly with the property of interest values (Table 5). The same holds for the RDKit attributor, although its overall performance on the test set is noticeably lower except for the standard deviation in the constant part (Table 5).

When examining example MMPs (Fig. 5), it becomes evident that the explainability methods fail to correctly localize the specific structural changes within the respective MMPs. This observation aligns with the high standard deviation found in the constant part, indicating inconsistent attributions. Given that aliphatic halides are well-known toxicophores for AMES mutagenicity,<sup>27</sup> one would expect the model to consistently highlight these regions, as shown in Fig. 5 (top MMP). However, the low correlation coefficient on the mutagenicity itself already suggests that the model struggles to capture and predict the relevant toxicophores, resulting in poor generalization to unseen data. The same holds true for aromatic amines (Fig. 5, middle and bottom), which are also established mutagenic motifs.<sup>27</sup> This stands in contrast to the work by Vangala *et al.*, whose Grad-CAM-based explainability approach correctly highlighted these key fragments.<sup>28</sup> Accurately identifying such critical substructures would be essential for enabling clear, chemistry-guided decision-making.

## 4 Overall trends

WISP allowed us to quantify the capabilities of the different explainability methods considered in this work (Table 5). Our results show that the newly developed, model- and descriptor-

agnostic atom attributor overall performs comparably—and especially more universally—than the SHAP or RDKit attributors.

The analysis of WISP with respect to the Crippen log $P$  dataset in part I demonstrates how effective these explanations can be:<sup>15</sup> the performance of the explainability of the variable part of the MMPs on the training set reaches an  $r^2$  of 0.79 and 0.77 on the test set. The machine learning model can explain unseen data with an  $r^2$  of up to 0.64 with respect to the whole molecule. This indicates that the explainability methods are already capable of addressing the challenge of explaining future data, but there is still significant room for improvement in model quality. In general, explaining unseen data remains challenging: only two of the eight evaluated experiments (Crippen log $P$  and solubility) show potential for successful application to future data when considering the whole molecule. This is a new finding compared to the work of Jiménez-Luna *et al.*, where no method was able to color previously unseen activity cliffs correctly.<sup>29</sup> However, for many of the tested endpoints, the explanations for predictions on the training set perform well.

Through the insights provided by WISP, users can also evaluate the predictive performance of their models by identifying regions where the model fails to learn the structure–property relationship accurately. This is demonstrated for the LCAP yield dataset (Section 3.2) and enables users to actively improve the model by including relevant data, thereby enhancing both predictive performance and explainability.

Based on the data presented in Table 5, we developed an action guide to help interpret the outputs of WISP (Fig. 6). Here, the correlation of each metric with the  $r^2$  on the test set provides perspective on its impact. An example correlation is shown in the SI (Fig. SI-4). This metric's impact was incorporated into the action guide (Fig. 6). Since the action guide is derived from the datasets used in this study, the cutoffs should not be interpreted as strict thresholds but rather as general guidelines. Users are advised to adjust these values according to the specific requirements of their application.

The primary indicator of explainability quality is the underlying model performance, as discussed in the first part of this series.<sup>15</sup> When the model demonstrates sufficient predictive quality, gaps in explainability performance can reveal specific model limitations, as exemplified by the LCAP yield dataset (Section 3.2). In general, we recommend evaluating the dataset at hand using a combination of the different metrics provided. The standard deviation of the constant part itself appears to be a qualitative indicator of explainability performance. When ranking the experiments by this metric on the training set, the resulting order aligns well with the qualitative impressions given by the heatmaps. This indicates that if WISP calculates a standard deviation of the constant part around 5 or higher, the resulting heatmaps should be interpreted with caution—particularly when the  $r^2$  value shows that the explainability performance on the property of interest is also low. Each metric focuses on a different aspect of explainability performance—whether it quantifies how well the model explains its predictions or the property of interest, and whether it assesses the whole molecule, the variable part, or the constant part. This

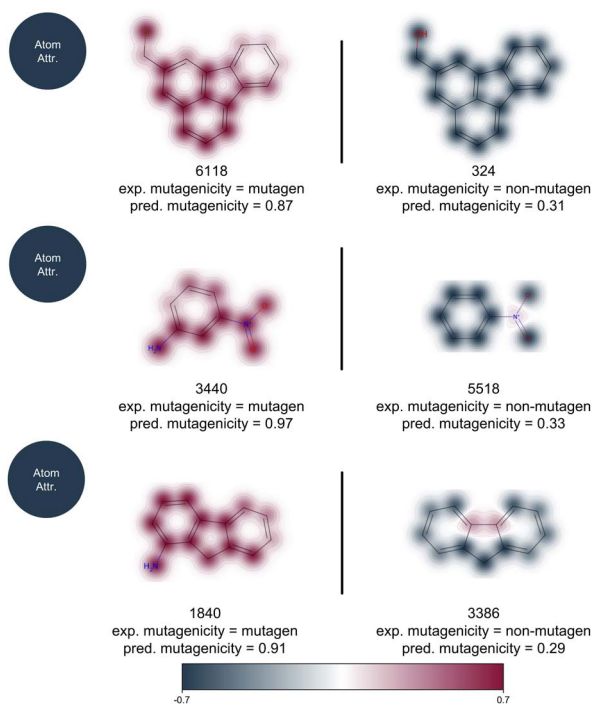


Fig. 5 Comparison of the heatmaps for different MMPs from the AMES mutagenicity dataset, generated using the atom attributor within WISP and scaled uniformly for consistency.



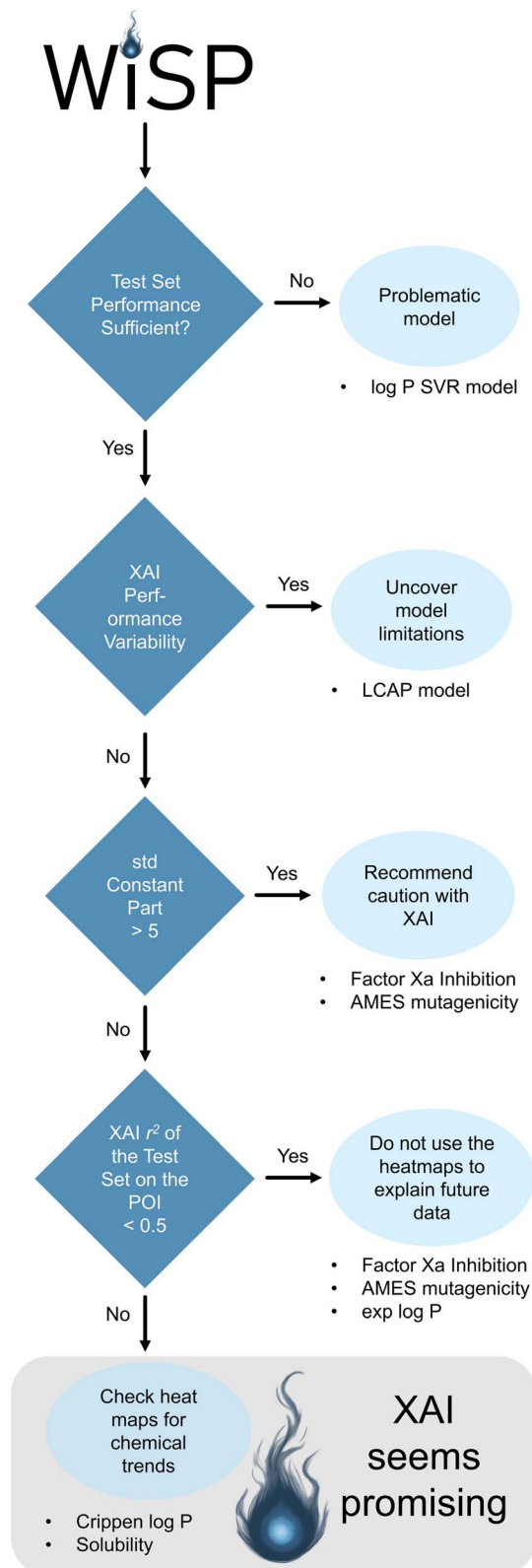


Fig. 6 Action guide for evaluating WISP results (POI = property of interest).

combination can help to identify cases where the explanations may be unreliable, allowing WISP to flag such datasets and support more robust decision-making.

## 5 Conclusion

By systematically applying WISP to a diverse range of datasets—including the Crippen log  $P$ , experimental log  $P$ , aqueous solubility, LCAP yield, Factor Xa  $pK_i$ , and AMES mutagenicity—we demonstrated that the performance of model explanations can be systematically quantified and benchmarked for both simple and complex structure–property relationships using matched molecular pairs. The generally applicable atom attributor performs comparably to less widely applicable methods like RDKit's SimilarityMaps and SHAP in many scenarios, providing robust, transferable explanations.

Furthermore, WISP exposes the limitations of current machine learning models in capturing subtle functional group effects, especially in challenging tasks like mutagenicity or bioactivity prediction, where non-additive and context-dependent interactions are critical.

Importantly, our findings emphasize that explaining predictions for unseen data remains a significant challenge: while on several datasets the explainability methods perform well on training data, only a few demonstrate the consistency and generalizability required for trustworthy predictions on new molecules. This underlines the necessity for rigorous dataset curation and continuous improvement of both models and explanation techniques.

## Author contributions

JMW and AHG: conceptualization, KJ and JMW: data curation, KJ: formal analysis, JP and AHG: funding acquisition, KJ: investigation, KJ and JMW: methodology, JP and AHG: project administration, JP and AHG: resources, KJ and JMW: software, JMW, JP and AHG: supervision, KJ: validation, KJ: visualization, KJ: writing – original draft, JMW, JP and AHG: writing – review & editing.

## Conflicts of interest

There are no conflicts to declare.

## Data availability

All code associated with this work, including the URL to the public web application, is available on GitHub at <https://github.com/kerjans/ml-XAI>. An archived version of the complete codebase is additionally accessible *via* Zenodo at <https://doi.org/10.5281/zenodo.17055142>.

Supplementary information (SI) is available. See DOI: <https://doi.org/10.1039/d5dd00399g>.

## Acknowledgements

JP acknowledges funding by Germany's joint federal and state program supporting early-career researchers (WISNA) established by the Federal Ministry of Research, Technology and Space (BMFTR). The authors acknowledge Philipp Held (TU Braunschweig) for providing explanatory Jupyter Notebooks on



WISP. In preparing this work, the authors used ChatGPT (OpenAI) to refine wording and provide coding assistance. All AI-generated material was thoroughly reviewed and edited by the authors, who assume full responsibility for the accuracy and integrity of the final publication.

## References

- 1 E. N. Muratov, J. Bajorath, R. P. Sheridan, I. V. Tetko, D. Filimonov, V. Poroikov, T. I. Oprea, I. I. Baskin, A. Varnek, A. Roitberg, O. Isayev, S. Curtalolo, D. Fourches, Y. Cohen, A. Aspuru-Guzik, D. A. Winkler, D. Agrafiotis, A. Cherkasov and A. Tropsha, *Chem. Soc. Rev.*, 2020, **49**, 3525–3564.
- 2 L. Zhang, J. Tan, D. Han and H. Zhu, *Drug Discovery Today*, 2017, **22**, 1680–1685.
- 3 K. Jorner, A. Tomberg, C. Bauer, C. Sköld and P.-O. Norrby, *Nat. Rev. Chem.*, 2021, **5**, 240–255.
- 4 J. Jiménez-Luna, M. Skalic, N. Weskamp and G. Schneider, *J. Chem. Inf. Model.*, 2021, **61**, 1083–1094.
- 5 C. Humer, H. Heberle, F. Montanari, T. Wolf, F. Huber, R. Henderson, J. Heinrich and M. Streit, *J. Cheminf.*, 2022, **14**, 21.
- 6 A. Chatzimpampas, R. M. Martins, I. Jusufi and A. Kerren, *Inf. Visual.*, 2020, **19**, 207–233.
- 7 P. Polishchuk, *J. Chem. Inf. Model.*, 2017, **57**, 2618–2639.
- 8 Y. Sushko, S. Novotarskyi, R. Körner, J. Vogt, A. Abdelaziz and I. V. Tetko, *J. Cheminf.*, 2014, **6**, 48.
- 9 G. Marcou, D. Horvath, V. Solov'ev, A. Arrault, P. Vayer and A. Varnek, *Mol. Inf.*, 2012, **31**, 639–642.
- 10 M. Matveieva and P. Polishchuk, *J. Cheminf.*, 2021, **13**, 41.
- 11 K. Janssen and J. Proppe, *J. Chem. Inf. Model.*, 2025, **65**, 1862–1872.
- 12 M. Eckhoff, J. V. Diedrich, M. Mücke and J. Proppe, *J. Phys. Chem. A*, 2024, **128**, 343–354.
- 13 J. Jiménez-Luna, F. Grisoni and G. Schneider, *Nat. Mach. Intell.*, 2020, **2**, 573–584.
- 14 L. Rosenbaum, G. Hinselmann, A. Jahn and A. Zell, *J. Cheminf.*, 2011, **3**, 11.
- 15 K. Janssen, J. M. Wollschläger, J. Proppe and A. H. Göller, *Digital Discovery*, 2025, submitted.
- 16 C. Tyrchan and E. Evertsson, *Comput. Struct. Biotechnol. J.*, 2017, **15**, 86–90.
- 17 S. Felten, C. Q. He, M. Weisel, M. Shevlin and M. H. Emmert, *J. Am. Chem. Soc.*, 2022, **144**, 23115–23126.
- 18 M. Bailey, S. Moayedpour, R. Li, A. Corrochano-Navarro, A. Kötter, L. Kogler-Anele, S. Riahi, C. Grebner, G. Hessler, H. Matter, M. Bianciotto, P. Mas, Z. Bar-Joseph and S. Jager, Deep Batch Active Learning for Drug Discovery, *bioRxiv*, 2023, DOI: [10.1101/2023.07.26.550653](https://doi.org/10.1101/2023.07.26.550653).
- 19 K. Hansen, S. Mika, T. Schroeter, A. Sutter, A. Ter Laak, T. Steger-Hartmann, N. Heinrich and K.-R. Müller, *J. Chem. Inf. Model.*, 2009, **49**, 2077–2081.
- 20 H. Heberle, L. Zhao, S. Schmidt, T. Wolf and J. Heinrich, *J. Cheminf.*, 2023, **15**, 2.
- 21 G. P. Wellawatte, H. A. Gandhi, A. Seshadri and A. D. White, *J. Chem. Theory Comput.*, 2023, **19**, 2149–2160.
- 22 T. Harren, H. Matter, G. Hessler, M. Rarey and C. Grebner, *J. Chem. Inf. Model.*, 2022, **62**, 447–462.
- 23 S. M. Lundberg and S.-I. Lee in *Advances in neural information processing systems*, ed. I. Guyon, U. V. Luxburg, S. Bengio, H. Wallach, R. Fergus, S. Vishwanathan and R. Garnett, Curran Associates, Inc., 2017, vol. 30.
- 24 S. Riniker and G. A. Landrum, *J. Cheminf.*, 2013, **5**, 43.
- 25 P. Schwaller, A. C. Vaucher, T. Laino and J.-L. Reymond, *Machine Learning: Science and Technology*, 2021, **2**, 015016.
- 26 V. Voinarovska, M. Kabeshov, D. Dudenko, S. Genheden and I. V. Tetko, *J. Chem. Inf. Model.*, 2024, **64**, 42–56.
- 27 J. Kazius, R. McGuire and R. Bursi, *J. Med. Chem.*, 2005, **48**, 312–320.
- 28 S. R. Vangala, S. R. Krishnan, N. Bung, R. Srinivasan and A. Roy, *J. Chem. Inf. Model.*, 2023, **63**, 5066–5076.
- 29 J. Jiménez-Luna, M. Skalic and N. Weskamp, *J. Chem. Inf. Model.*, 2022, **62**, 274–283.

